Spectrochimica Acta Part B: Atomic Spectroscopy 229 (2025) 107198

Contents lists available at ScienceDirect

Spectrochimica Acta Part B: Atomic Spectroscopy

journal homepage: www.elsevier.com/locate/sab

Online analysis of coal particle flow by laser-induced breakdown spectroscopy based on pelletized coal calibration samples and feature-based transfer learning☆

Meirong Dong [a,c], Zhichun Li [a,b], Junbin Cai [a,c], Weiye Lu [b], Xiaoxuan Chen [a,b], Kaijie Bai [b], Shunchun Yao [a,c,*], Jidong Lu [a,c]

[a] School of Electric Power Engineering, South China University of Technology, Guangzhou, Guangdong 510640, China
[b] Guangdong Institute of Special Equipment Inspection and Research Shunde Branch, Foshan 528300, China
[c] Guangdong Province Engineering Research Center of High Efficient and Low Pollution Energy Conversion, Guangzhou, Guangdong 510640, China

ARTICLE INFO

Keywords:
Coal properties
On-line analysis
LIBS
Particle flow
Feature-based transfer learning

ABSTRACT

The application of laser-induced breakdown spectroscopy (LIBS) for directly measuring coal particle flow is an optimal choice for the actual industrial operations. With the objective of facilitating the detection of particle flow, we established a LIBS detection system coupled with the coal particle circulation bench, which can continuously and automatically provide particle flow samples for laser ablation. A quantitative analysis method for particle flow combining feature-based transfer learning was proposed, so a dual-mode optical LIBS module was designed and integrated into this system to obtain the spectral signals from different forms of coal samples (pellet and particle flow) through the same optical configuration. The spectral characteristics and the correlation between pellet and particle flow were firstly analyzed. Then a spectral correction method based on polynomial fitting was proposed to enhance the correlation between the pellet spectra and particle flow spectra. Finally, the feature space mapping method was introduced for improving the effect of feature transfer, and the model was trained on highly stable pellet spectra to perform a direct quantitative analysis of coal particle flow. The results demonstrated that the root mean square error (RMSE) for the analysis of calorific value, volatile matter, and ash content of particle flow was 0.757 MJ/kg, 2.630 %, and 3.034 %, respectively. This work provides a practical application scheme for on-line analysis of coal particle flow.

1. Introduction

As an important primary energy source, coal is widely used in the power industry [1,2]. It is of great significance to realize the accurate and rapid analysis of coal components and characteristics for improving energy utilization efficiency and reducing pollutant emissions [3,4]. Traditional coal analysis methods, such as thermogravimetric analysis (TGA), are difficult to use for real-time analysis as they require a time-consuming treatment process [5]. Prompt gamma neutron activation analysis (PGNAA) [6] has been used as a feasible technology for on-line monitoring of coal, but the measurement system is often bulky, expensive, and involves radiation hazards. Laser-induced breakdown spectroscopy (LIBS) is an in-situ rapid analysis technique based on atomic emission spectroscopy [7,8], with the advantages of wide sample applicability, minimally destructive, multi-element measurement, and so on [9–11], which has been applied in various fields including geochemistry [12], mineral exploration [13], medicine [14] and space exploration [15].

LIBS has been applied in coal property analysis since 1991 by Ottesen et al. [16]. They applied LIBS to determine the composition of coal (C, H, and O). Since then, a number of studies have been carried out, and LIBS technology has emerged as a promising new method for the detection of coal quality. Wang et al. [17,18] proposed a method for standard spectra combined with the partial least squares regression, effectively improving the accuracy and repeatability of LIBS measurements of coal composition. Mateo et al. [19,20] analyzed the influence of operation modes and laser wavelengths on the compositional characteristic of coal and evaluated the determination of combustion predictive indices of

☆ This article is part of a Special issue entitled: 'LIBS2024' published in Spectrochimica Acta Part B: Atomic Spectroscopy.

* Corresponding author at: School of Electric Power Engineering, South China University of Technology, Guangzhou, Guangdong 510640, China.
E-mail address: epscyao@scut.edu.cn (S. Yao).

https://doi.org/10.1016/j.sab.2025.107198
Received 28 December 2024; Received in revised form 22 March 2025; Accepted 26 March 2025
Available online 27 March 2025
0584-8547/© 2025 Elsevier B.V. All rights are reserved, including those for text and data mining, AI training, and similar technologies.

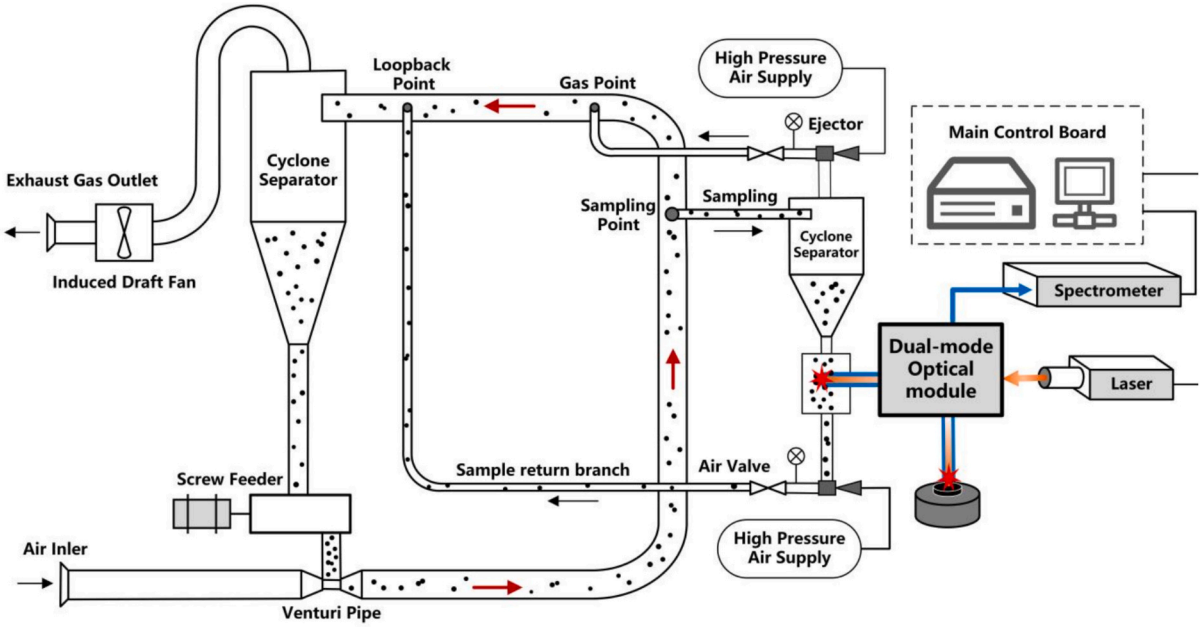

Fig. 1. Schematic diagram of the LIBS measurement system with coal particle circulation bench.

coals and coal blends. Zhang et al. [21,22]used particle swarm optimization (PSO) and internal standard methods to process spectral data and improve accuracy. Our previous work conducted a series of investigations to address the mechanism of laser ablation of coal samples [23,24], and the improvement method in quantitative analysis of coal properties was proposed [25,26]. Most of the above research including the fundamental study and optimization of data-mining methods are based on coal pellet samples.

At present, in order to develop a LIBS system for on-site coal analysis in the power plants [27,28], the main sample forms are as follows: (i) compressing coal particles into pellets for detection [29], (ii) detecting the coal rocks moving on the conveyor belt [30], (iii) directly detecting the coal particle flow [31]. It is well known that in most coal-fired power plants, coal is delivered to the burner in the form of gas-solid powder two-phase flow. Therefore, the direct measurement of coal particle flow sampling for the pipe is considered to be the most suitable scheme for online analysis, which can avoid the complicated sample preparation process, with better measurement representativeness. However, due to the spatial density inhomogeneity and randomness of the particle flow, there are fluctuations in the interaction process between the laser and the coal particles [32], which would cause poor repeatability and weak spectral stability [33]. In our previous work, we have already conducted some works to study and optimize LIBS particle flow detection and found that the tapered tube with a diameter of 5.5 mm was particularly useful to enrich the coal particles in laser focus spot [34]. Yu et al. [35] has investigated the plasma morphology fluctuation due to stochastic particle ablation in LIBS particle flow analysis and reported that air-prominent and extreme plasma presented more repeatable signals due to less plasma morphology fluctuation. Chen et al. [36] proposed a spectral data screening method based on plasma image information to identify the effective LIBS spectrum from coal particle flow, improving the accuracy of particle flow measurement. Cai et al. [37] used particle flow cylindrical spatial confinement schemes and spectral screening to optimize the quantitative analysis performance of coal particle flow.

It is widely acknowledged that a considerable number of studies have been performed with the objective of analyzing coal particle flow. Nevertheless, the technical challenge of achieving on-site and online analysis of coal particle flow persists, with notable difficulties in maintaining stability and calibrating the system. In comparison, the laser ablation process of coal pellets is stable due to its smooth and compact surface, and its spectroscopy has higher stability and repeatability [38,39]. Therefore, our group is committed to proposing a novel measurement scheme that integrates the stability of the coal pellet detection mode and the convenience of the particle flow mode. The scheme has been tested on the powder feeder experimental bench [40]. By investigating the similarity of the spectral properties in the coal pellet and particle flow, a quantitative analysis model incorporating both data based on the transfer learning method, which has been shown to yield reliable results.

The concept of transfer learning has been developed on the basis of traditional machine learning algorithms. The effectiveness of traditional machine learning models is contingent upon the statistical homogeneity of the train data sets (source domain data) and testing data sets (target domain data), however, through transfer learning, the differences in data features between the target domain and the source domain are permitted [41,42]. Feature-based transfer learning, a subset of transfer learning, optimizes knowledge utilization across domains by altering data distributions and transforming features. [43,44]. It has been widely applied in the field of spectral detection and analysis. Shabbir et al. [45,46] introduced a feature and instance-based transfer learning method, which improved the prediction performance of LIBS model for surface irregular metals by effectively correcting physical matrix effects, demonstrating the effectiveness of transfer learning to overcome physical matrix effects caused by changes in sample physical states. Hu et al. [47] studied the application of transfer learning algorithm in Raman spectroscopy detection of pesticide residues and improved the model accuracy and speed of feature extraction and classification using three different transfer learning models. Sun et al. [48] studied the LIBS physical matrix effect caused by different surface states between powder particles and rocks, and introduced transfer learning algorithms in data processing. They used laboratory compression sample training models to predict the original rock spectra. In summary, transfer learning techniques are an effective means of extracting and integrating data features, and are applicable to a multitude of scenarios, including those pertaining to LIBS analysis.

At present, most research on coal particle flow measurement by LIBS is conducted with powder feeders producing particle flow. In order to better simulate the pipeline condition of coal-fired power plants, the coal particle circulation bench and the gas-solid two-phase flow sampling setup were established. Furthermore, to better achieve

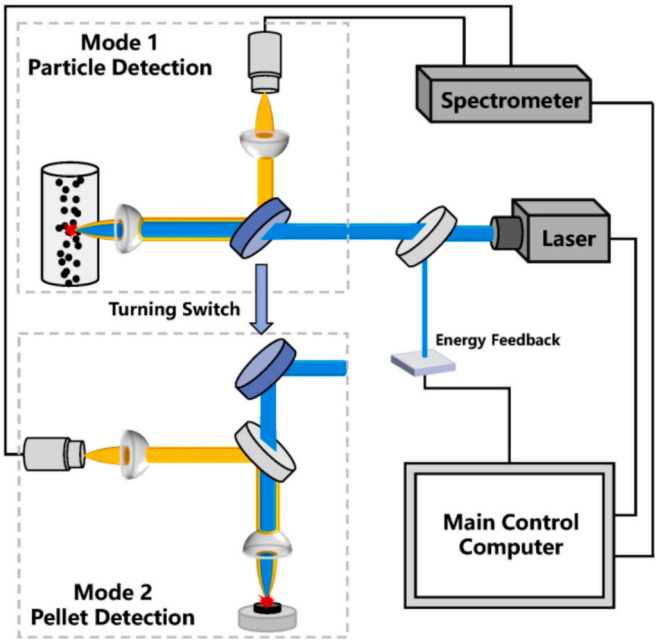

Fig. 2. The dual-mode optical LIBS module for the detection of coal pellet and particle flow.

quantitative analysis of coal particle flow, a dual-mode LIBS detection equipment for coal pellet and particle flow was developed. Then a novel LIBS calibration scheme was proposed for the prediction of coal particle flow properties by combining spectroscopic data from coal pellet samples through the feature-based transfer learning method.

2. Experimental

2.1. Coal particle circulation bench

In pulverized coal-fired boilers, the coal sample is transported to the boiler burner in the form of a particle stream by pneumatic conveyance. In order to simulate the scenario in the coal-fired power plant, we established a coal particle circulation bench, as shown in Fig. 1. This bench mainly includes cyclone separators, spiral powder feeders, induced draft fans, Venturi tubes, air compressors, air valves, and other essential components. The induced draft fan situated behind the cyclone separator provides a dynamic for the circulation flow system. Consequently, the entire air-particle pipeline is in a negative pressure state, whereby ambient air enters the system from the inlet to the Venturi pipe and is mixed with the coal particles falling from the feeder. The two-phase air-particle flow enters the cyclone separator along the pipeline, where the coal particles and air are separated. The exhaust gas is discharged from the upper part, and the coal particles fall back into the feeder storehouse by gravity. Additionally, the screw feeder can regulate the mass flow within the pipeline.

A bypass device for continuous sampling and return was constructed, including sampling tube, injectors, cyclone separators, air compressors, regulating valves, and other components. This configuration enables the device to perform continuous automatic sampling and feedback. Upon initiation of the sampling system, the air compressor and regulating valves will be activated, thereby providing dynamic support for the sampling injector. The negative pressure effect generated by the sampling injector causes the coal particles in the main pipeline to flow out of the sampling tube (shaped like a piccolo) and into the cyclone separator in the measurement section. After the two-phase separation of the gas and solid phases, the gas returns to the main pipe, while the coal particles descend into the LIBS measurement chamber. A reflux device has been designed so that the particles are then returned to the circulation pipeline under the action of the injector, preventing accumulation issues and eliminating the need for manual cleaning.

2.2. LIBS detection system

In order to achieve the objective of employing stable pellet spectral data to assist particle flow detection, it is necessary to ensure the effective acquisition of LIBS data for both forms of the sample under identical optical settings. We developed a dual-mode LIBS measurement cabinet, which incorporates an integrated optical circuit, for measuring coal particle flow and pellets. The configuration of the internal optical path is illustrated in Fig. 2. In the particle flow measurement mode

Table 1
The representative proximate analysis index of the coal samples.

Sample No.	Volatile matter (wt%)	Ash content (wt%)	Calorific value (MJ/kg)	Sample No.	Volatile matter (wt%)	Ash content (wt%)	Calorific value (MJ/kg)
A1	29.92	14.08	20.84	A26	34.47	7.63	22.02
A2	19.04	48.16	11.13	A27	19.86	22.54	22.79
A3	34.72	14.82	13.70	A28	26.68	15.22	21.98
A4	40.27	15.66	18.90	A29	24.4	15.65	22.42
A5	25.56	15.76	21.92	A30	26.77	18.29	24.50
A6	29.47	13.86	26.16	A31	23.27	18.88	22.39
A7	23.72	41.08	17.16	A32	20.9	17.82	23.39
A8	27.44	19.50	22.04	A33	20.62	19.66	25.3
A9	28.54	15.22	19.00	A34	16.16	25.52	23.64
A10	13.10	73.96	4.62	A35	26.39	23.38	21.9
A11	37.16	17.88	15.39	A36	16.11	34.56	17.1
A12	32.04	15.44	18.88	A37	21.25	28.97	19.50
A13	13.49	32.78	22.48	A38	32.32	14.45	17.27
A14	28.60	21.18	23.62	A39	34.71	7.98	23.50
A15	40.11	2.52	20.82	A40	23.79	31.69	15.07
A16	29.31	13.44	26.18	B1	27.91	14.04	19.42
A17	14.40	42.64	17.24	B2	4.92	23.13	25.00
A18	13.74	29.60	22.35	B3	27.93	4.06	24.05
A19	13.83	33.18	20.98	B4	39.99	8.06	21.40
A20	19.14	32.84	19.44	B5	16.26	36.22	16.28
A21	22.58	13.24	22.52	B6	16.42	40.43	17.66
A22	17.10	19.81	24.47	B7	6.50	18.90	27.15
A23	15.8	23.98	21.59	B8	2.58	37.30	19.32
A24	18.94	27.46	22.1	B9	10.10	31.52	19.87
A25	28.03	15.05	23.11	B10	28.28	20.96	23.8

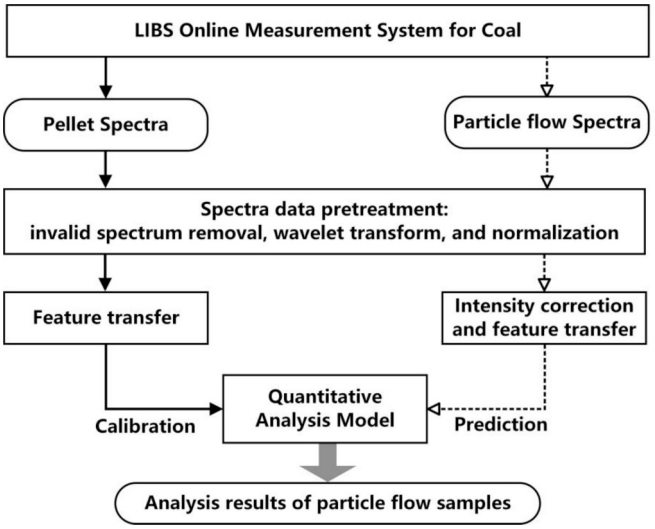

Fig. 3. The flowchart of spectral data acquisition, processing and model.

(Mode 1), the pulsed laser emitted by the pulse laser passes through a 45°mirror, with 99 % of the light transmitted directly and only approximately 1 % reflected into the silicon detector, thus enabling laser energy monitoring. The transmitted light is then focused and irradiated on the surface of the coal particle flow through a dichroic mirror and a combination lens, resulting in the generation of the particle flow plasma. The plasma emission is reflected by the dichroic mirror to the receiving system, where it is focused by the flat convex lens and transmitted to the spectrometer through optical fibers.

In the other mode (Mode 2), designed for pellet measurement, the pulsed laser is reflected by the laser reflector and enters the apparatus vertically. Subsequently, the laser beam traverses the transmission surface of the dichroic mirror and is then focused by the flat convex lens, before being directed towards the surface of the pellet sample. The plasma emissions are reflected to the receiving system by the dichroic mirror reflection surface.

In this work, the laser source was generated by a Nd: YAG pulsed laser (Brilliant Easy, Quantel, France), whose operating wavelength was 1064 nm and the pulse width was 6 ns. To reduce mutual interference, the laser pulse frequency was set to 2 Hz between pulses while maintaining efficiency. The laser energy was set to 65 mJ after pre-experimental optimization. A focusing lens with a diameter of 25.4 mm and a focal length of 50 mm was employed to focus the laser pulse to the center of the particle flow or the surface of the pellet and generate plasma. To effectively excite coal particles, the spot size at the laser focusing point is adjusted to 250 μm. The plasma emission was collected to the six-channel spectrometer (Netherlands Avantes, AvaSpec-ULS2048CL), which covers a spectral range of 170–870 nm with a resolution of about 0.09–0.28 nm. The delay time from the laser output trigger signal to spectrometer scanning and the gate width was set to 600 ns and 1.1 ms, respectively.

2.3. Specimen preparation

In this experiment, 50 coal samples collected from power plants were employed as experimental samples. Following grinding and sieving, coal powders with a particle size of less than 200 μm were obtained and placed in a 45 °C oven for 4 h to facilitate air drying. The representative proximate analysis index of all samples is shown in Table 1. The calorific value is determined by the bomb calorimetric method, and the measurement error is around ±0.2 %. The volatile matter and ash content are determined by thermogravimetric analysis, and the measurement error is around ±0.5 %. Prior to the experiment, each coal sample was weighed at 3.5 g and then pressed into a 25 mm diameter pellet under a pressure of 6.5 t for 20 s. The spectral data recorded for each particle flow sample comprised 500 pulses, while that recorded for each pellet sample comprised 9 positions, with 20 pulses per position, resulting in a total of 180 pulses. Ten samples (B1-B10) were randomly selected as the particle flow samples, and the remaining 40 samples (A1-A40) were used as the pellet samples. Pellet data were gathered from 40 samples (A1-A40) as the train set for the model. Both pellet and particle flow spectra were collected from 10 samples (B1-B10) for the purpose of conducting a spectral characteristic analysis and model validation.

3. Methods

Fig. 3 illustrates the flowchart of spectral data analysis, processing, and model construction. Following the acquisition of spectral data, the spectral characteristics of pellet and particle flow were firstly analyzed. Subsequently, a spectral correction method based on polynomial fitting was proposed. Finally, the feature space mapping method was introduced for improving the effect of feature transfer, and the model was trained on highly stable pellet spectra to perform a direct quantitative analysis of coal particle flow. A detailed introduction to methods is given below.

3.1. Spectral analysis and intensity correction

To better quantitatively analyze the spectral correlation between particle flow samples and pellet samples, the Pearson correlation coefficient ρ was used to evaluate the degree of linear correlation between spectra.

$$\rho(a,b) = \frac{Cov(a,b)}{\sqrt{Var(a)} \times \sqrt{Var(b)}} \tag{1}$$

where $\rho(a,b)$ is Pearson correlation, $Cov(a,b)$ is the covariance between pellet data and particle flow data, $Var(a)$ is the variance. The Pearson coefficient was used to describe the degree of linear correlation between two variables, and the larger the coefficient, the higher the linear correlation.

The polynomial fitting function is a commonly used method for correcting data differences [49]. There are significant spectral intensity differences between particle flow data and pellet data at different wavelength pixels. To improve the spectral correlation, we proposed a spectral intensity correction method based on the polynomial fitting function. It aimed to find a suitable functional relationship between pellet spectra and particle flow spectra. Assuming the following formula holds at different wavelength ranges:

$$\varphi[I(\lambda)] = I^*(\lambda) = a_0 + a_1 I(\lambda) + a_2 I^2(\lambda) + \cdots + a_k I^k(\lambda) \tag{2}$$

where $a_0, a_1, a_2, \ldots, a_k$ are undetermined parameters for polynomial, k is the maximum degree of fit terms, $I(\lambda)$ is the original intensity of particle flow spectrum at the wavelength pixel λ, $I^*(\lambda)$ is the corrected spectral intensity.

Assuming there are n sets of fitted data, the above formula can be written in the following matrix form:

$$\begin{bmatrix} 1 & I_1(\lambda) & \cdots & I_1^k(\lambda) \\ 1 & I_2(\lambda) & \cdots & I_2^k(\lambda) \\ \vdots & \vdots & \ddots & \vdots \\ 1 & I_n(\lambda) & \cdots & I_n^k(\lambda) \end{bmatrix} \begin{bmatrix} a_0 \\ a_1 \\ \vdots \\ a_k \end{bmatrix} = \begin{bmatrix} I_1^*(\lambda) \\ I_2^*(\lambda) \\ \vdots \\ I_n^*(\lambda) \end{bmatrix} \tag{3}$$

Parameters $a_0, a_1, \ldots, a_k$ can be estimated with least squares solution by minimizing the error of the corrected particle flow spectral intensity and the pellet spectral intensity [50,51]. After selecting the appropriate k for the highest degree term, the coefficient matrix can be calculated from the above formula, to correct the spectral intensity. When the highest degree term is a single term ($a_1 \neq 0$, $a_2 = a_3 = \ldots = a_k = 0$), it is

linear fitting. And if $k = 2$, it is quadratic fitting. The fitting function of high-order terms is prone to over-fitting and requires large computation amount, so we selected linear fitting correction (LFC) and quadratic fitting correction (QFC) to improve spectral correlation between particle flow spectra and pellet spectra.

3.2. Feature space mapping

In order to better apply the spectral data from coal pellet to the prediction of particle flow, feature transfer learning (FTL) based on space mapping was employed. The idea feature space mapping is to find a mapping function ϕ, so that the target domain data Y_j has better similarity with the source domain data X_i in the new feature space. To avoid both performing explicit nonlinear mappings and computing dot products in the feature space, the kernel function is a widely used method for feature space mapping [52,53]:

$$\kappa\left(x_i, y_j\right) = \left\langle \phi(x_i), \phi\left(y_j\right) \right\rangle \tag{4}$$

where κ is the kernel function, $\phi(x_i)$ is the mapping function, $\langle , \rangle$ represents the inner product operation. This work chose the Gaussian function as the kernel function κ, as shown in Formula 5:

$$\kappa\left(x_i\ ,\ y_j\right) = exp\left(-\frac{\| x_i - y_j\|^2}{2\sigma^2}\right) \tag{5}$$

where, x and y are the spectral data of two samples, and σ is kernel bandwidth.

To fully utilize the information in the spectral bands, before performing kernel function calculation, the full spectrum data $X_i^{[\lambda_{min},\lambda_{max}]}$ is divided into N segments ($X_i^{[\lambda_1,\lambda_2]}$, $X_i^{[\lambda_2,\lambda_3]}$, …, $X_i^{[\lambda_N,\lambda_{N+1}]}$). Then perform kernel function calculations for each segment of data:

$$\kappa^*\left(x_i\ ,\ y_j\right) = \left[\kappa^{[\lambda_1,\lambda_2]}\left(x_i\ ,\ y_j\right), \ldots, \kappa^{[\lambda_N,\lambda_{N+1}]}\left(x_i\ ,\ y_j\right)\right] \tag{6}$$

where $\kappa^{[\lambda_1,\lambda_2]}\left(x_i\ ,\ y_j\right)$represents the kernel function of data in the wavelength range[λ_1,λ_2], $\lambda_1 = \lambda_{min}$, $\lambda_{N+1} = \lambda_{max}$, and $\kappa^*\left(x_i\ ,\ y_j\right)$ represents the kernel function after segmentation. As the spectrometer used in the experiment was 6-channel, the spectrum was divided into six corresponding segments.

3.3. Model establishment

3.3.1. Spectral data pretreatment

The LIBS spectral acquisition process is susceptible to a number of environmental factors, which can result in the generation of invalid-excited or weak-excited spectral data, especially for particle flow detection. The signal-to-noise ratio (SNR) method is a common method used for single-frame spectrum screening [54], as following calculation formula:

$$SNR = \frac{X - \overline{X_i}}{\sqrt{\frac{\sum_{i=1}^{n}(X_i - \overline{X_i})^2}{n-1}}} \tag{7}$$

where X is the spectral line intensity of characteristic element, n is the number of adjacent spectral lines near the characteristic peek, X_i is the background intensity, $\overline{X_i}$ is the average intensity of the background.

In optical measurement, high-frequency noise in the spectral signals can interfere with the useful information. The wavelet transform (WT) is an effective method [55] for improving signal-to-noise ratio. The WT of a spectral signal, which describes the energy at any wavelength-frequency point, is defined as follows:

$$W(w,f) = \int_{-\infty}^{\infty} I(\lambda)\frac{1}{\sqrt{f}}\phi^*\left(\frac{\lambda - w}{f}\right)d\lambda \tag{8}$$

where $\phi(x)$ is the mother wavelet, and ϕ*(x)is the complex conjugate of $\phi(x)$. This work used the threshold method to effectively remove noise signals.

Normalization can help eliminate dimensional differences, unify data scales, and facilitate subsequent analysis and model construction. So normalization processing was conducted to convert the spectra to dimensionless form. The relative intensity of spectra for the whole wavelength can be calculated as the following calculation formula:

$$I^*(\lambda) = \frac{n\, I(\lambda)}{\sum_{\lambda-w}^{\lambda+w} I(\varphi)} \tag{9}$$

where $I(\lambda)$ is the original spectral intensity at the wavelength pixel λ, $I(\varphi)$ is the spectral intensity at each wavelength pixel within the wavelength range $(\lambda - w, \lambda + w)$, and n is the number of spectral data within the range.

For spectral feature selection, the standard deviation (SD) was used to evaluate the importance of spectra data dimensions [56,57]. The calculation formula is as follows:

$$SD_\lambda = \sqrt{\frac{\sum_{i=1}^{n}(y_{\lambda i} - \widehat{y}_\lambda)^2}{n-1}} \tag{10}$$

where SD_λ represents the spectra data standard deviation of all samples at wavelength pixel λ, n is the number of samples, $y_{\lambda i}$ represents the spectral intensity of sample i at wavelength pixel λ, $\widehat{y}_\lambda$ is the average intensity at wavelength pixel λ.

In order to enhance the representativeness of the spectral data, the pretreated spectra of each sample were divided into 5 groups, then the average spectra of each group were calculated for model training and testing.

3.3.2. Analysis model and evaluation parameters

The partial least squares regression (PLSR) is a multivariate data analysis method that is widely used in the field of spectral analysis [58]. This work used partial least squares regression as the quantitative analysis model.

The determination coefficient R^2, root mean square error (RMSE), and mean relative error (MRE) were used to evaluate the predictive performance of model. Their calculation formulas are as follows:

$$R^2 = \frac{\sum_{i=1}^{n}(\widehat{y}_i - \overline{\widehat{y}})(y_i - \overline{y})}{\sqrt{\sum_{i=1}^{n}(\widehat{y}_i - \overline{\widehat{y}})^2 (y_i - \overline{y})^2}} \tag{11}$$

$$RMSE = \sqrt{\frac{1}{n-1} \bullet \sum_{i=1}^{n}(y_i - \widehat{y}_i)^2} \tag{12}$$

$$MRE = \frac{1}{n}\sum_{i=1}^{n}\frac{|y_i - \widehat{y}_i|}{y_i} \tag{13}$$

where y_i and $\widehat{y}_i$ represent the actual test reference value and model prediction value of the sample i, $\overline{y}$ and $\overline{\widehat{y}}$ represent the average of the actual test reference value and model prediction value of the sample set. And n is the number of data set.

4. Results and discussion

4.1. Pellet and particle flow spectral analysis

4.1.1. Identification of effective breakdown spectra of coal particle flow

It is well known that the breakdown conditions and plasma properties are very different for the coal particle flow and the pellet. In the

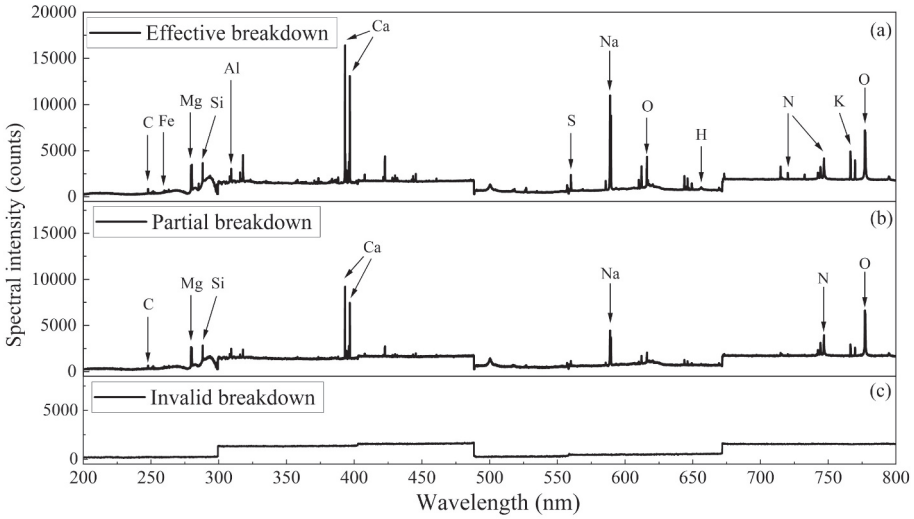

Fig. 4. Typical particle flow spectra of coal#B1 for each excitation state: (a) effective breakdown; (b) partial breakdown; (c) invalid breakdown.

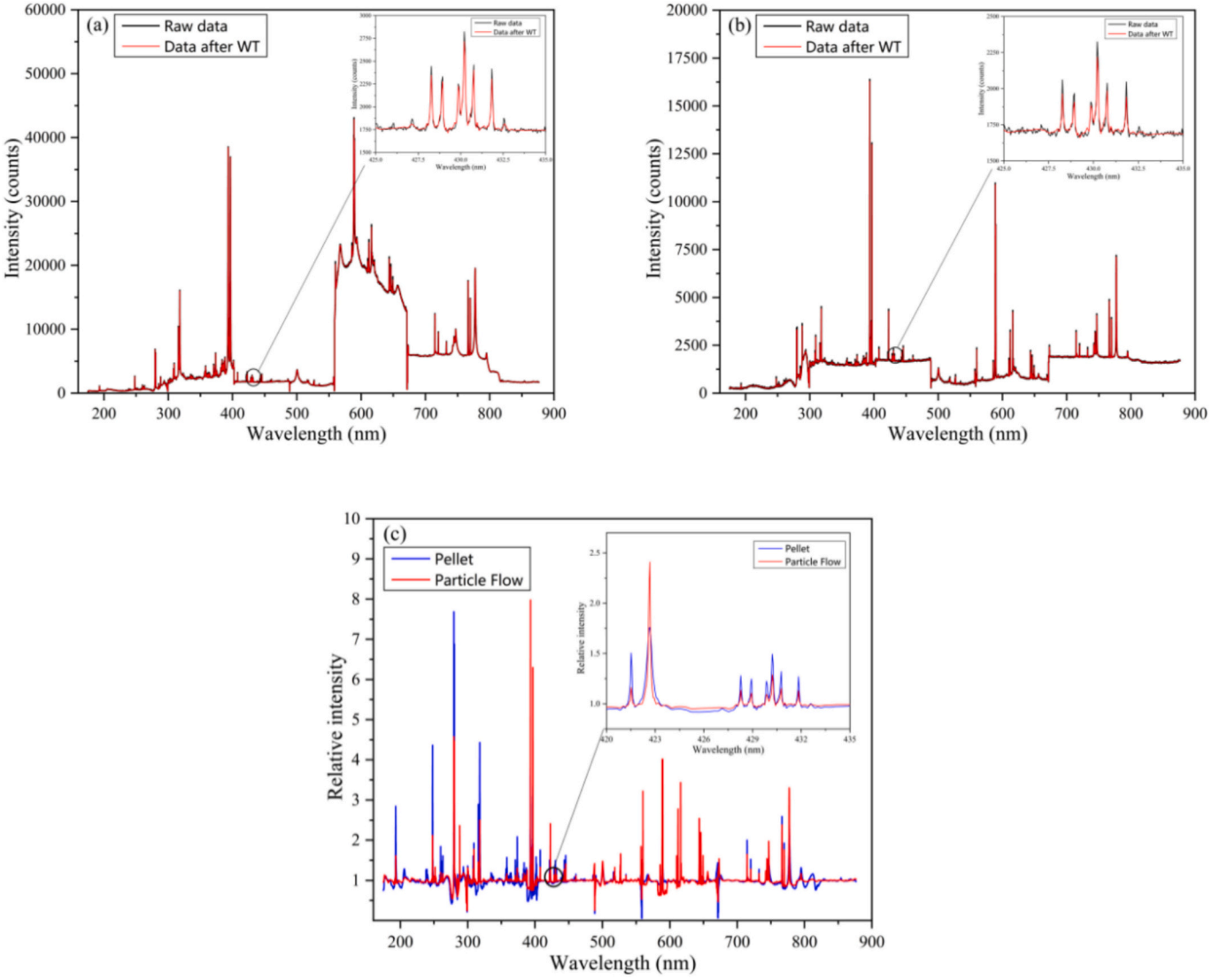

Fig. 5. Spectral data before and after processing of coal sample #B1 (a) pellet spectrum after WT; (b) particle flow spectrum after WT; (c) spectra after normalization.

Table 2
The correlation analysis of raw spectral data.

Spectral correlation	Sample#B1 Pellet	Sample#B1 Particle flow	Other Samples Pellet	Other Samples Particle flow
Sample#B1 Pellet	≥ 0.99	0.60–0.70	0.90–0.97	0.59–0.66
Sample#B1 Particle flow	0.60–0.70	≥ 0.98	0.52–0.62	0.70–0.95

pellet case, particles on the surface of solid samples can be stably broken down, ablated, and generate plasma. Most of the emitters in the plasma originate from the sample components. It is worth to mention that coal particles in this experiment were observed to be around 200 μm in size, with the 150–200 μm fraction constituting the predominant component. This is significantly larger than the typical range of ordinary aerosols (0.1–100 μm). The motion of particles in the flow is primarily governed by gravity, friction, and collisions. The concentration of particles in the gas-solid flow is about 30 g/min, which differs from the aerosol detection by LIBS. Therefore, in the case of particle flow detection, the characteristic of plasma emission is dependent on the concentration of particle flow. While the spatial density of particles in the flow beam is not kept constant, which is the main reason for the low spectral intensity and low stability of particle flow. Therefore, in coal particle flow analysis, the LIBS spectrum obtained when a sufficient number of particles are broken down is referred to as the effective breakdown spectra, as illustrated in Fig. 4.

As illustrated in Fig. 4, there are instances of partial and invalid breakdown spectra, which are deemed to be inadequately representative and should be eliminated [59]. Carbon is the primary component of coal (usually 50 %- 90 %), and the atomic emission line of carbon serves as a clear indication of the excitation state. In the SNR method, the C I 247.86 nm line is frequently selected for identifying the effective breakdown spectra from laser-induced particle flow samples [60]. When setting the SNR threshold, both the quality of the spectral data and the quantity of the spectral data must be considered. A low SNR value is not conducive to removing invalid data, while a high SNR value will remove too much data. The threshold for SNR is therefore set at 3.5. Approximately 8 % of the particle flow spectra were then considered to be invalid or weak and were therefore excluded from further analysis.

4.1.2. *Spectral characteristics from the coal pellet and particle flow samples*

Fig. 5(a)(b) shows the typical spectrum of coal sample # B1 under different physical states. Compared to particle flow, the spectral line intensity of the pellet spectrum was generally much higher. The characteristic peaks of pellet spectra were more stable and prominent compared to the particle flow spectra, so the information of characteristic elements was accurate and clear. This is mainly due to the fact that

Table 3
Model prediction results after intensity correction.

Coal Indicators	PLSR		PLSR-LFC		PLSR-QFC	
	RMSE	MRE	RMSE	MRE	RMSE	MRE
Volatile matter	10.251	85.37 %	6.759	68.15 %	6.686	32.91 %
Ash content	8.825	88.25 %	5.935	49.10 %	5.404	42.32 %
Calorific value	3.535	13.75 %	1.989	7.98 %	2.405	10.63 %

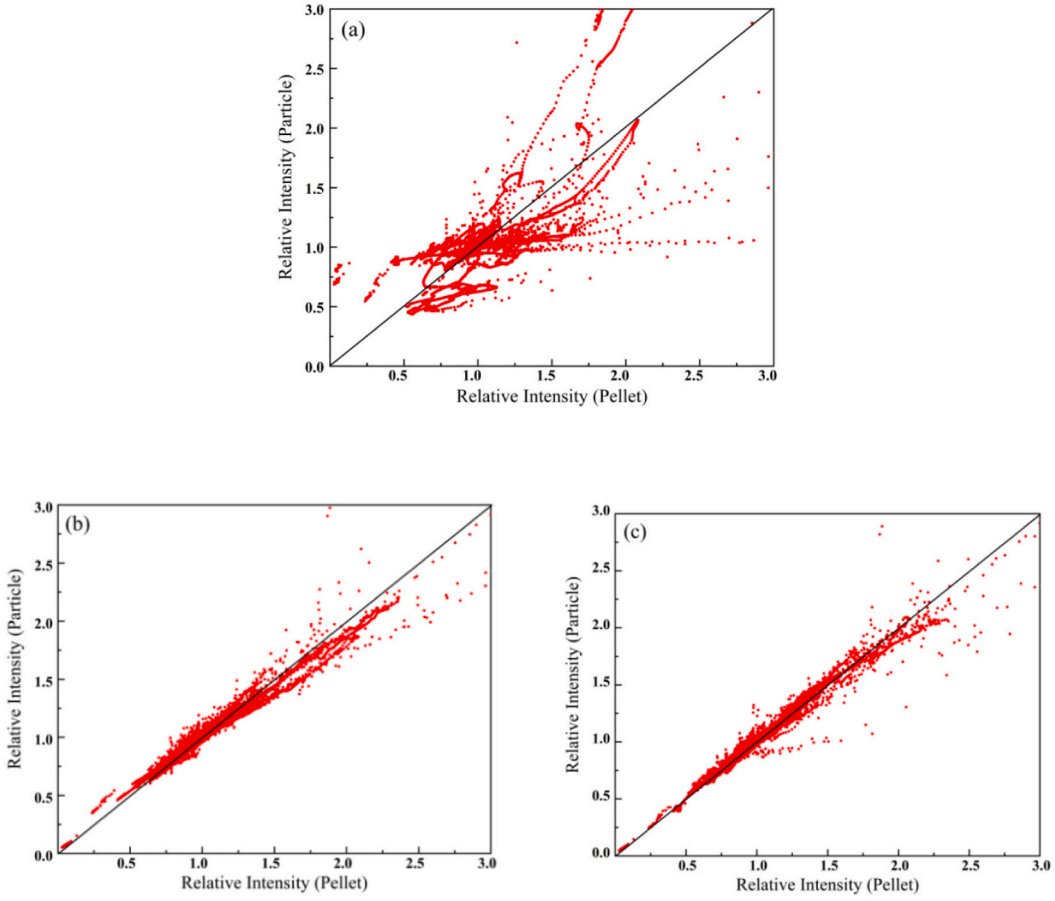

Fig. 6. Spectral line intensity plot of pellet and particle flow samples: (a) without correction; (b) linear fitting correction; (c) quadratic fitting correction.

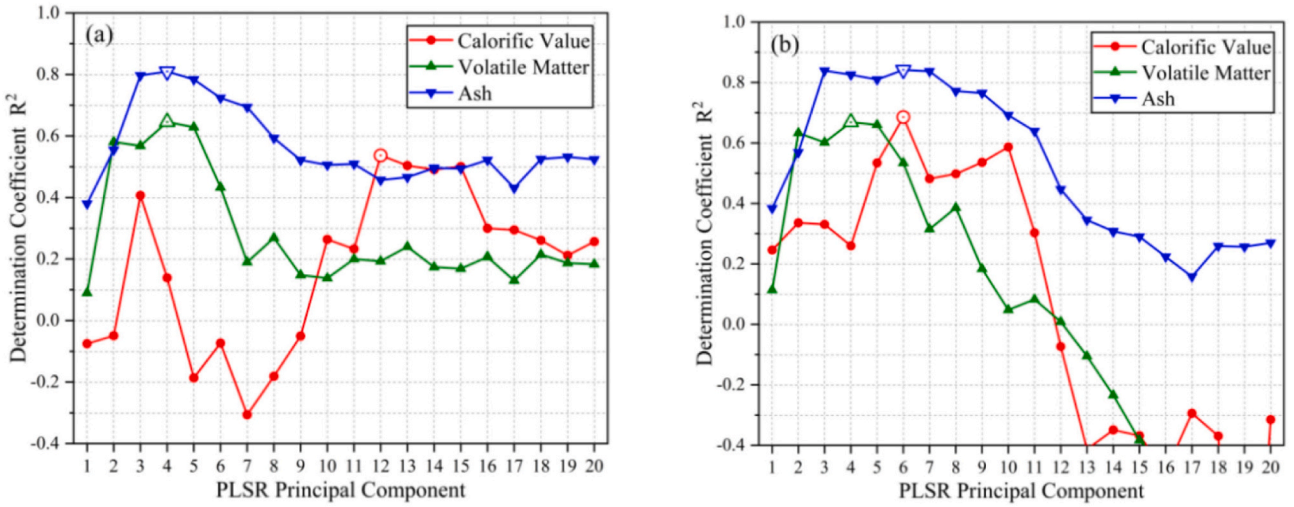

Fig. 7. Prediction performance of the model at different component. (a) PLSR - LFC (b) PLSR - QFC.

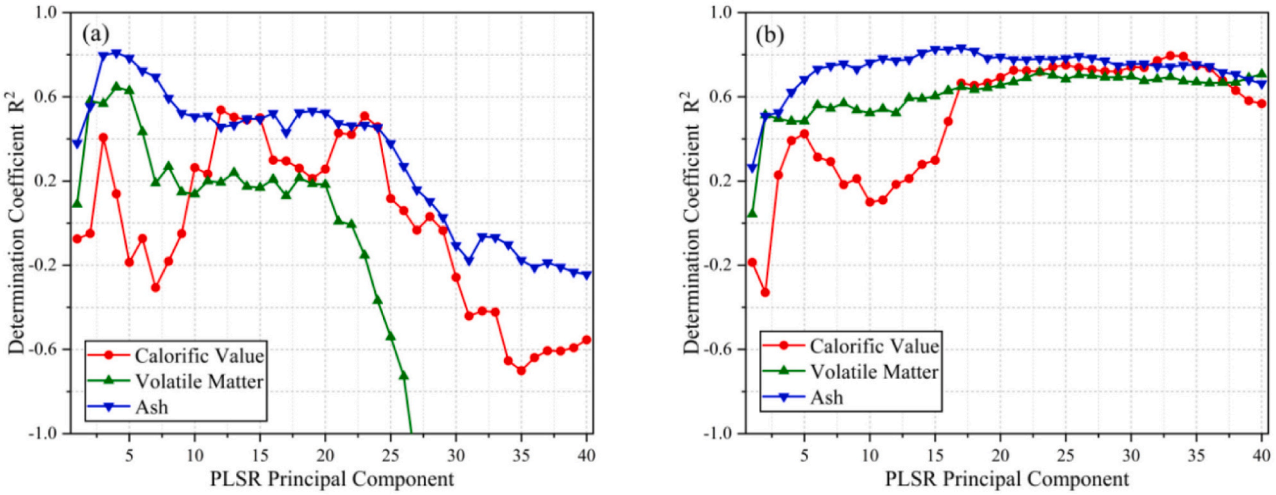

Fig. 8. The quantitative results with and without feature space mapping: (a) model with LFC; (b) model with LFC - FSM.

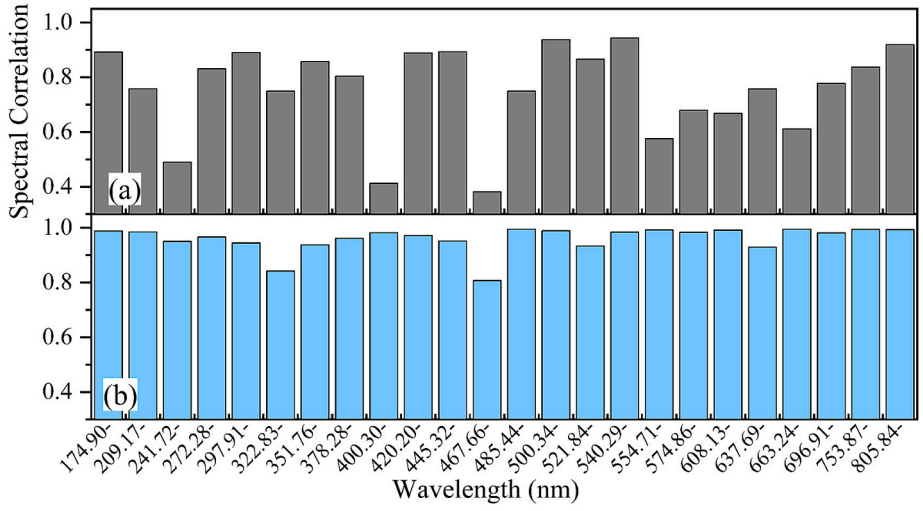

Fig. 9. The spectral correlation between particle flow spectra and pellet spectra in different wavelength ranges: (a) Without LFC; (b) with LFC.

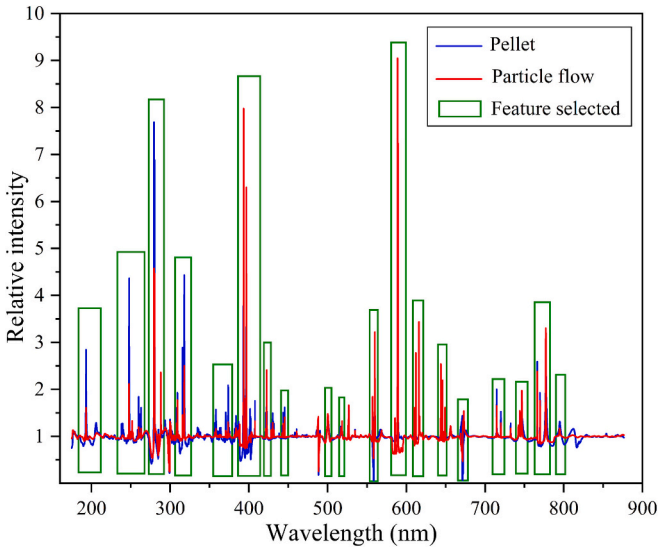

Fig. 10. The spectral features favored for selection.

Table 4
The comparison of model prediction performance.

Coal indicators	PLSR-LFC-FSM			
	Without feature selection		With feature selection	
	R^2	RMSE	R^2	RMSE
Calorific value	0.795	1.322	0.947	0.757
Volatile matter	0.797	3.659	0.920	2.630
Ash content	0.833	5.564	0.936	3.034

the coal particle spatial density of the flow beam is much lower than that of the compact surface of the pellets, leading to less ablation on the flow beam and less substance being ionized. On the other hand, the coal particle flow beam contains gas, which weakens the airflow and impedes the transfer of energy between particles. Significant background noise was observed in two types of spectra. Thus, the wavelet transform (WT) was used to reduce spectral background noise. It can be seen that after WT, the spectral background noise was reduced and the spectral lines became smoother. In the same frequency domain, the atomic characteristic spectral lines of laser induced plasma exhibit narrow spectral line width and large peak amplitude values, while the noise signal presents a wider and lower characteristic compared to the atomic characteristic spectral line. WT can effectively decompose spectral signal data into different dimensions without causing significant changes in the shape of spectral lines, thereby extracting the high-frequency and low-frequency components of spectral signals.

Additionally, we can see in Fig. 5(a)(b) that there are differences in the background intensity of pellet and particle flow spectra, in particular, that of the pellet spectra in the 558 nm -671 nm wavelength range was quite intense. To unify data scales, the spectral data after WT were normalized. As shown in Fig. 5(c), the disparity in background signals between each channel was markedly diminished, and the characteristic spectral lines became more pronounced in the whole spectrum.

4.1.3. Correlation analysis between the spectra of pellet and particle flow

The correlation between spectral data from different physical states was analyzed before features transfer learning. It should be noted that particle flow spectral data are not statistically equivalent to the pellets' spectral data due to the different physical states involved. The correlation is an important factor determining the effectiveness of transfer learning. Taking sample#B1 as an example, the spectral correlation between different physical states was analyzed, as well as the correlation between #B1 and other samples, as shown in Table 2.

It can be seen that for the same coal sample and physical state, the correlation between spectra is relatively high, reaching more than 0.98. For the same physical state, the correlation between different coal samples in the pellet sample spectrum was above 0.9 and had a small fluctuation range, while the inter-sample correlation of the particle flow spectrum had a larger fluctuation range, between 0.7 and 0.95. This indicated that the stability of the particle flow spectrum was lower. For the same coal sample, under different physical states, the correlation between the pellet spectrum and particle flow spectrum was only 0.6–0.7, showing that the physical state was more significant to the spectral correlation.

4.2. Feature transfer learning model for coal particle flow analysis

4.2.1. Influence of spectral intensity correction

To improve the spectral correlation between particle flow spectra and pellet spectra, linear fitting correction (LFC) and quadratic fitting correction(QFC) methods were adopted to correct the spectral intensity. The relationship between particle flow data and pellet data was illustrated on the scatter plot in Fig. 6.

It was evident that in the absence of correction, the spectral intensity scatter distribution of samples exhibiting disparate physical states was characterized by a high degree of chaos and disorder. Following correction, the spectral intensity scatter points were concentrated towards the diagonal and distributed on both sides of the diagonal, indicating that the similarity and correlation between both kinds of spectra were greatly improved.

Table 3 lists the model prediction results after spectral intensity correction. Traditional machine learning models require the train set and the test set to have the same or similar distribution, otherwise, there is a risk of model failure. The excitation states and matrix effects generated by laser strikes on pellet samples and particle flow samples are different, leading to differences in the spectral data characteristics, so the model trained by pellet spectra cannot make accurate predictions for the original particle flow spectra. It can be seen that after the intensity correction of particle flow data, the predictive performance of the model constructed using pellet data has been improved.

Compared to linear fitting, quadratic fitting correction provided better numerical approximation, resulting in superior model prediction performance. However, as the number of principal components increased, the model with QFC demonstrated significantly greater instability in its prediction performance in comparison to the model with LFC. Fig. 7 shows the model prediction performance in different principal components. The number of principal components is a key hyperparameter in the PLSR model, determining its ability to capture and explain the variance within the training data. The pellet data was input as training set data into the PLSR model, so the principal components determining the explanatory capability for pellet data. At low components (7–9), the PLSR-QFC demonstrated strong predictive performance for particle flow data, achieved by sacrificing the calibration model's explanatory capability for pellet data. When component numbers exceed 10, the PLSR-LFC model outperformed the PLSR-QFC model, but significant fluctuations in the prediction performance of particle flow are observed for both models, indicating that the feature transfer learning effect between particle flow data and pellet data has not yet been fully realized.

4.2.2. Quantitative analysis results optimized by feature space mapping

After intensity correction, the feature space mapping method was introduced to improve the effect of feature transfer. Both LFC and QFC methods manifested nearly prediction accuracies, but the LFC method demonstrated superior stability, so the ensuing discussions would be based on the LFC method. Fig. 8 presents a comparative analysis of the quantitative results with and without feature space mapping.

It is evident that following the implementation of feature space

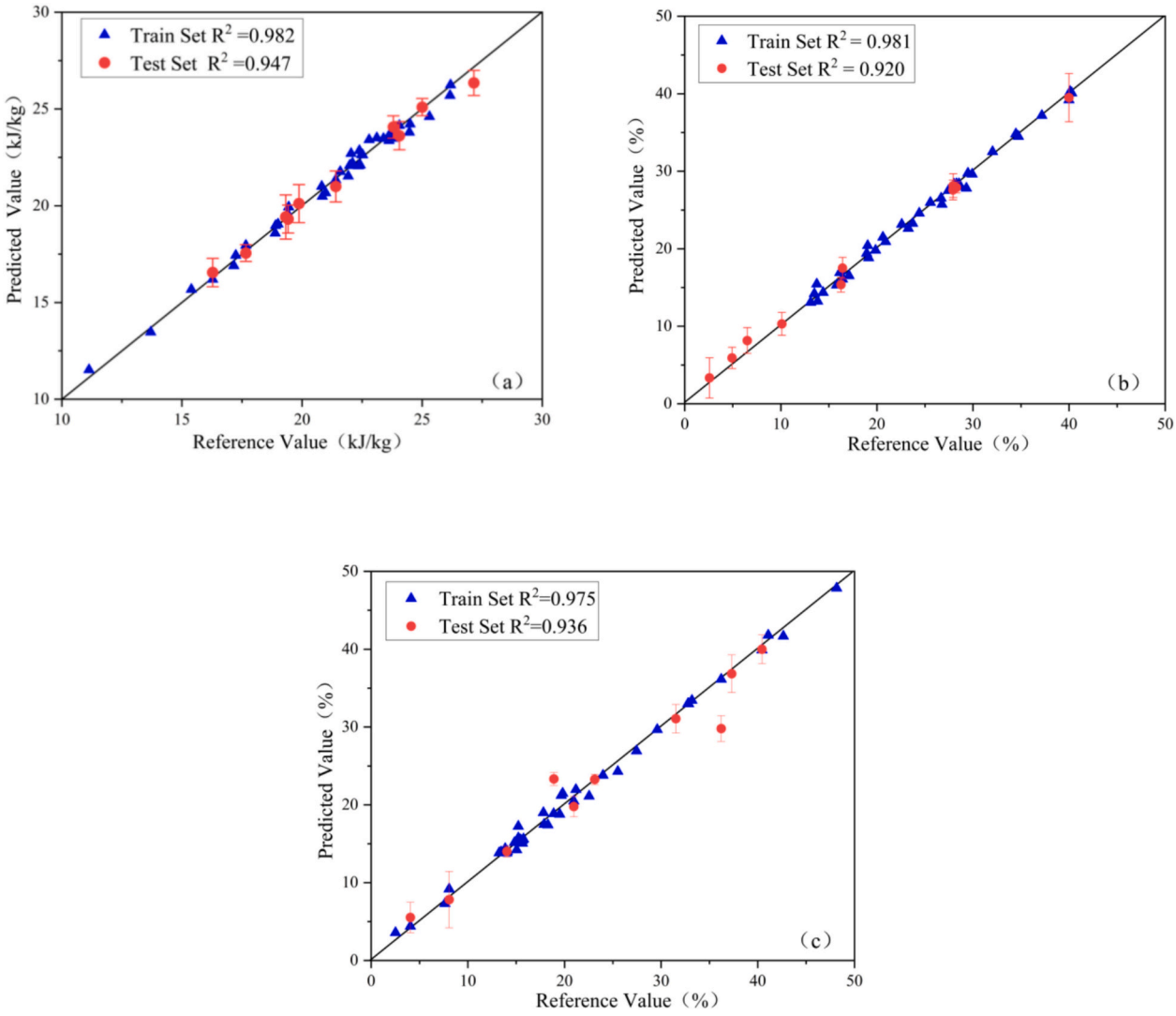

Fig. 11. Quantitative analysis result after spectral feature selection. (a) calorific value (b) volatile matter (c) ash content.

mapping, the predictive performance of the model was further improved. As the number of components increased, the model with FSM maintained its calibration capability for pellet data while exhibiting both accuracy and stability in the predictive performance of particle flow data. This demonstrated effective feature transfer between particle flow data and pellet data. The feature space mapping method based on kernel function not only improved the feature similarity between different domain data but also extracted the distance information between samples and transferred it to the regression model, thereby enhancing the effectiveness of transfer learning.

4.2.3. Further improvement of model performance by feature selection

Feature selection is a widely used and effective method for improving the predictive performance of machine learning models, and can also be combined with feature transfer learning. To improve the effectiveness of feature transfer learning, feature selection was undertaken with consideration for both spectral similarity and information richness.

The spectral data in this experiment contained more than 12,000 pixels. To better analyze the spectral correlation between particle flow spectra and pellet spectra in different features, every 500 consecutive pixel were divided into one section, with the first segment spanning 174.90–209.17 nm, the second spanning 209.17 nm–241.72 nm, and so forth, as shown in Fig. 9.

It can be seen that the spectral correlation varied greatly in different segments, and spectral correlation has been improved significantly after LFC with the correlation of some segments (174.90–209.17 nm, 485.44–500.34 nm, 554.71–574.86 nm, 608.13–637.69 nm, 663.24–696.91 nm, 753.87–805.84 nm) approaching 0.99. This further demonstrated the effectiveness of intensity correction in improving the similarity of spectral data. And spectral features with high correlation are more likely to be selected.

The standard deviation(SD) is selected as the evaluation index for data information richness [56,57], which is a statistical measure that is used to describe the degree of dispersion of the data set. In this study, the standard deviation (SD) of spectral intensities across all pellet samples was calculated for each wavelength pixel. This process enabled the identification of spectral features exhibiting low SD values were identified as redundant and thus suitable candidates for elimination. Therefore, a basis for spectral feature screening has been obtained. By integrating the aforementioned two considerations, the spectral features obtained after the selection are shown in Fig. 10.

Then the spectra after feature selection were used for the model with LFC-FSM, and the results are shown in Table 4 and Fig. 11. Compared to the model without feature selection, the model with feature selection demonstrates significantly enhanced prediction performance. Specifically, the determination coefficients R^2 for calorific value, volatile matter, and ash content in particle flow test data all exceeded 0.90,

while the root mean square errors were reduced to 0.757 MJ/kg, 2.630 %, and 3.034 %, respectively. Normally, the spectra obtained by the spectrometer cover a broad range of wavelengths and high-dimensional spectra often contain redundant spectral information, which can hinder model calibration and prediction performance. Through feature selection, the spectral features that facilitate feature transfer and model construction can be identified, significantly enhancing the model's performance.

5. Conclusions

Direct measurement of particle flow is considered to be the most suitable method for online analysis of coal properties by using LIBS. This study aims to propose a measurement scheme that can be better suited for the actual condition of the power plant. Firstly, a LIBS measurement device in conjunction with the coal particle circulation bench was developed. The objective was to construct a system that would enable a continuous sampling and return of coal particle flow. In order to detect the spectral characteristics of coal samples in different physical states, a dual-mode optical LIBS module was developed. Subsequently, the spectral characteristics of particle flow and pellet samples were analyzed. The results showed that the spectral stability of the pellet was superior to that of the particle flow spectrum, and a correlation between the two types of spectra was identified. According to the characteristics of particle flow spectra and pellet spectra, a spectral intensity correction method based on polynomial fitting was proposed, which effectively improved the spectral correlation. The quantitative analysis model was trained by pellet data for directly predicting particle flow, and the feature space mapping method was introduced to improve the effect of feature transfer. Finally, the predictive performance of the model was further improved through feature selection. The RMSE for the calorific value, volatile matter, and ash content were improved to 0.757 MJ/kg, 2.630 %, and 3.034 %, respectively. The use of machine learning algorithm can further improve their correlation between the spectra from pellets and particle flow, thereby serving as an auxiliary enhancement for predictive methods by integrating and leveraging the two types of spectral data. Nevertheless, it should be noted that the spectral data obtained from pellets is unable to fully capture the complete properties of the particle flow, and that transfer learning cannot alter the intrinsic properties of the particle flow itself. Further optimization of particle flow measurement requires in-depth exploration of its fundamental characteristics.

CRediT authorship contribution statement

Meirong Dong: Writing – review & editing, Resources, Project administration, Conceptualization. **Zhichun Li:** Writing – review & editing, Writing – original draft, Visualization, Validation, Methodology, Data curation. **Junbin Cai:** Writing – review & editing, Methodology, Conceptualization. **Weiye Lu:** Supervision, Formal analysis. **Xiaoxuan Chen:** Investigation, Data curation. **Kaijie Bai:** Software, Investigation. **Shunchun Yao:** Supervision, Project administration, Methodology. **Jidong Lu:** Supervision.

Declaration of competing interest

The authors declare that they have no known competing financial interests or personal relationships that could have appeared to influence the work reported in this paper.

Acknowledgement

The research was supported by National Natural Science Foundation of China (No. 52376107 & U22B20119), Foundation of Science and Technology Projects in Guangzhou (2025A04J7048). and the Fundamental Research Funds for the Central Universities (2022ZFJH004). We also acknowledge the support from Guangdong Province Key Laboratory of Efficient and Clean Energy Utilization (2013A061401005) and Project of Guangdong Institute of Special Equipment Inspection and Research (2024CY-2-06).

Data availability

Data will be made available on request.

References

[1] H. Schobert, C. Song, Chemicals and materials from coal in the 21st century, Fuel 81 (2002) 15–32, https://doi.org/10.1016/S0016-2361(00)00203-9.
[2] J. Yang, Y. Yu, T. Ma, et al., Evolution of energy and metal demand driven by industrial revolutions and its trend analysis, Chin. J. Popul., Resour. Environ. 19 (2021) 44–52, https://doi.org/10.1016/j.cjpre.2021.12.028.
[3] P. Nelson, P. Shah, V. Strezov, B. Halliburton, J.N. Carras, Environmental impacts of coal combustion: a risk approach to assessment of emissions, Fuel 89 (2010) 810–816, https://doi.org/10.1016/j. fuel.2009.03.002.
[4] K. Guo, Y. Li, J. Wang, et al., A review on selenium in coal-fired power plants: content and forms in coal, determination methods, migration, transformation, and control technologies, J. Environ. Chem. Eng. 8 (2006) 694–698, https://doi.org/10.1016/j.jece.2024.113579.
[5] Y. Zhang, Z. Xiong, Y. Ma, et al., Quantitative analysis of coal quality by laser-induced breakdown spectroscopy assisted with different chemometric methods, Anal. Methods 12 (2020) 3530–3536, https://doi.org/10.1039/d0ay00905a.
[6] B. Sowerby, Nuclear techniques for the on-line bulk analysis of carbon in coal-fired power stations, Appl. Radiat. Isot. 67 (2009) 1638–1643, https://doi.org/10.1016/j.apradiso.2009.04.007.
[7] L. Cabalin, T. Delgado, L. Garcia, J.J. Laserna, Considerations on formation mechanisms of emitting species of organic and C-containing inorganic compounds in CO_2 atmosphere using laser-induced breakdown spectroscopy as a strategy for detection of molecular solids, Spectrochim. Acta B At. Spectrosc. 169 (2020) 105869, https://doi.org/10.1016/j.sab.2020.105869.
[8] H. Jin, X. Hao, Y. Yang, Laser-induced breakdown spectroscopy combined with principal component analysis-based support vector machine for rapid classification of coal from different mining areas, Optik 286 (2023) 170990, https://doi.org/10.1016/j.ijleo.2023.170990.
[9] K. Liu, C. He, C. Zhu, et al., A review of laser-induced breakdown spectroscopy for coal analysis, Trends Anal. Chem. 143 (2021) 116357, https://doi.org/10.1016/j.trac.2021.116357.
[10] M. Gaft, T. Dvire, H. Modiano, et al., Laser induced breakdown spectroscopy machine for online ash analyses in coal, Spectrochim. Acta B 63 (10) (2008) 1177–1182, https://doi.org/10.1016/j. sab.2008.06.007.
[11] D. Palásti, A. Metzinger, T. Ajtai, et al., Qualitative discrimination of coal aerosols by using the statistical evaluation of laser-induced breakdown spectroscopy data, Spectrochim. Acta B At. Spectrosc. 153 (2019) 34–41, https://doi.org/10.1016/j.sab.2019.01.009.
[12] R.S. Harmon, G.S. Senesi, Laser-induced breakdown spectroscopy - a geochemical tool for the 21st century, Appl. Geochem. 128 (2021) 104929, https://doi.org/10.1016/j.apgeochem.2021.104929.
[13] R.S. Harmon, C.J. Lawley, J. Watts, C.L. Harraden, A.M. Somers, R.R. Hark, Laser-induced breakdown spectroscopy – an emerging analytical tool for mineral exploration, Minerals 9 (2019) 718, https://doi.org/10.3390/min9120718.
[14] A. Skalny, T. Korobeinikova, M. Aschner, et al., Medical application of laser-induced breakdown spectroscopy (LIBS) for assessment of trace element and mineral in biosamples: laboratory and clinical validity of the method, J. Trace Elem. Med. Biol. 79 (2023) 127241, https://doi.org/10.1016/j.jtemb.2023.127241.
[15] Y. Rao, C. Sun, X. Yu, et al., Precise chlorine determination in geological materials using LIBS coupled with stable learning for Mars explorations, Spectrochim. Acta B At. Spectrosc. 213 (2024) 106881, https://doi.org/10.1016/j.sab.2024.106881.
[16] D. Ottesen, L. Baxter, L. Radziemski, et al., Laser spark emission spectroscopy for in-situ, real-time monitoring of pulverized coal particle composition, Energy&Fuels 5 (1991) 304–312, https://doi.org/10.1021/ef00026a014.
[17] Z. Hou, Z. Wang, T. Yuan, et al., A hybrid quantification model and its application for coal analysis using laser-induced breakdown spectroscopy, J. Anal. At. Spectrom. 31 (2016) 722–736, https://doi.org/10.1039/c5ja00475f.
[18] Y. Lyu, W. Song, Z. Hou, et al., Incorporating empirical knowledge into data-driven variable selection for quantitative analysis of coal ash content by laser-induced breakdown spectroscopy, Plasma Sci. Technol. 26 (2024) 075509, https://doi.org/10.1088/2058-6272/ad370c.
[19] M.P. Mateo, G. Nicolas, A. Yanez, Characterization of inorganic species in coal by laser-induced breakdown spectroscopy using UV and IR radiations, Appl. Surf. Sci. 254 (2007) 868–872, https://doi.org/10.1016/j.apsusc.2007.08.043.
[20] T. Ctvrtnickova, M. Mateo, A. Yanez, G. Nicolas, Application of LIBS and TMA for the determination of combustion predictive indices of coals and coal blends, Appl. Surf. Sci. 257 (2011) 5447–5451, https://doi.org/10.1016/j.apsusc.2010.12.025.
[21] L. Zhang, J. Hou, Y. Zhao, et al., Investigation on accurate proximate analysis of coal using laser-induced breakdown spectroscopy, Spectrosc. Spectr. Anal. 37 (2017) 3198–3203, https://doi.org/10.3964/j.issn.1000-0593(2017)10-3198-06.

[22] X. Li, L. Zhang, Z. Tian, et al., Ultra-repeatability measurement of the coal calorific value by XRF assisted LIBS, J. Anal. At. Spectrom. 35 (2020) 2928–2934, https://doi.org/10.1039/D0JA00362J.
[23] M. Dong, X. Mao, J.J. Gonzalez, et al., Time-resolved LIBS of atomic and molecular carbon from coal in air, argon and helium, J. Anal. Atom. Spectrom. 27 (2012) 2066–2075, https://doi.org/10.1039/C2JA30222E.
[24] J. Cai, M. Dong, Y. Zhang, et al., Temporally and spatially resolved study of laser-induced plasma generated on coals with different volatile matter contents, Spectrochim. Acta B 180 (2021) 106195, https://doi.org/10.1016/j.sab.2021.106195.
[25] M. Dong, L. Wei, J. Lu, et al., A comparative model combining carbon atomic and molecular emissions based on partial least squares and support vector regression correction for carbon analysis in coal using LIBS, J. Anal. Atom. Spectrom. 34 (2019) 480–488, https://doi.org/10.1039/C8JA00414E.
[26] Y. Zhang, M. Dong, L. Cheng, et al., Improved measurement in quantitative analysis of coal properties using laser induced breakdown spectroscopy, J. Anal. Atom. Spectrom. 35 (2020) 810–818, https://doi.org/10.1039/C9JA00429G.
[27] M. Mateo, G. Nicolas, A. Yanez, Characterization of inorganic species in coal by laser-induced breakdown spectroscopy using UV and IR radiations, Appl. Surf. Sci. 254 (4) (2007) 868–872, https://doi.org/10.1016/j.apsusc.2007.08.043.
[28] S. Yao, J. Lu, M. Dong, et al., Extracting coal ash content from laser-induced breakdown spectroscopy (LIBS) spectra by multivariate analysis, Appl. Spectrosc. 65 (2011) 1197–1201, https://doi.org/10.1366/10-06190.
[29] Z. Wang, Y. Liu, R. Whiddon, et al., Measurement of atomic sodium release during pyrolysis and combustion of sodium-enriched Zhundong coal pellet, Combust. Flame 176 (2017) 429–438, https://doi.org/10.1016/j.combustflame.2016.10.020.
[30] D. Redoglio, E. Golinelli, S. Musazzi, et al., A large depth of field LIBS measuring system for elemental analysis of moving samples of raw coal, Spectrochim. Acta B At. Spectrosc. 116 (2016) 46–50, https://doi.org/10.1016/j.sab.2015.11.005.
[31] M. Dong, J. Cai, H. Liu, et al., A review of laser-induced breakdown spectroscopy and spontaneous emission techniques in monitoring thermal correction of fuels, Spectrochim. Acta B At. Spectrosc. 210 (2023) 106807, https://doi.org/10.1016/j.sab.2023.106807.
[32] Z. Wang, Y. Deguchi, M. Kuwahara, et al., Quantitative elemental detection of size-segregated particles using laser-induced breakdown spectroscopy, Spectrochim. Acta B At. Spectrosc. 87 (2013) 130–138, https://doi.org/10.1016/j.sab.2013.05.034.
[33] M. Afgan, S. Sheta, Y. Song, et al., Plasma imaging for physical variations in laser-induced aerosol plasma with particle size increase, J. Anal. At. Spectrom. 35 (2020) 2649–2655, https://doi.org/10.1039/d0ja00297f.
[34] S. Yao, J. Xu, X. Dong, et al., Optimization of laser-induced breakdown spectroscopy for coal powder analysis with different particle flow diameters, Spectrochim. Acta B At. Spectrosc. 110 (2015) 146–150, https://doi.org/10.1016/j.sab. 2015.06.011.
[35] Z. Yu, W. Ma, W. Chen, et al., Investigation on plasma morphology fluctuation in laser-induced breakdown spectroscopy analysis of particle flow due to stochastic particle ablation, Spectrochim. Acta B At. Spectrosc. 211 (2024) 106840, https://doi.org/10.1016/j.sab.2023.106840.
[36] Y. Chen, M. Dong, J. Cai, et al., An image auxiliary method for laser-induced breakdown spectroscopy analysis of coal particle flow, J. Anal. At. Spectrom. 37 (2022) 1126–1133, https://doi.org/10.1039/d2ja00023g.
[37] J. Cai, M. Dong, H. Chen, et al., An optimization method based on spatial confinement and spectra data screening for laser-induced breakdown spectroscopy quantitative analysis of coal particle flow, At. Spectrosc. 45 (2024) 200–208, https://doi.org/10.46770/AS.2024.092.
[38] Z. Yu, S. Yao, Y. Jiang, et al., Comparison of the matrix effect in laser induced breakdown spectroscopy analysis of coal particle flow and coal pellets, J. Anal. At. Spectrom. 36 (2021) 2473, https://doi.org/10.1039/D1JA00223F.
[39] M. Dong, L. Wei, J. Lu, et al., Quantitative analysis of LIBS coal heat value based on K-CV parameter optimization support vector machine, spectroscopy and spectral, Analysis 39 (2019) 2202–2209, https://doi.org/10.3964/j.issn.1000-0593(2019)07-2202 -08.
[40] Y. Chen, M. Dong, J. Cai, et al., Quantitative analysis of coal particle flow by laser induced breakdown spectroscopy based on tradaboost algorithm, Proc. Chin. Soc. Electri. Eng. 43 (24) (2024) 9638–9645, https://doi.org/10.13334/j.0258-8013.pcsee.221733.
[41] L. Xia, Z. Yang, W. Wei, et al., A rapid in-situ hardness detection method for steel rails based on LIBS and machine learning, Spectrochim. Acta B At. Spectrosc. 215 (2024) 106908, https://doi.org/10.1016/j.sab.2024.106908.
[42] T. Chen, T. Zhang, H. Li, Applications of laser-induced breakdown spectroscopy (LIBS) combined with machine learning in geochemical and environmental resources exploration, TrAC Trends Anal. Chem. 133 (2020) 116113, https://doi.org/10.1016/j.trac.2020.116113.
[43] Y. Li, K. He, D. Xu, D. Luo, A transfer learning method using speech data as the source domain for micro-Doppler classification tasks, Knowl.-Based Syst. 209 (2020) 106449, https://doi.org/10.1016/j.knosys.2020.106449.
[44] L. Dong, H. Shu, Z. Tang, et al., Microseismic event waveform classification using CNN-based transfer learning models, international journal of, Min. Sci. Technol. 33 (2010) 1203–1216, https://doi.org/10.1016/j.ijmst.2023.09.003.
[45] S. Shabbir, Y. Zhang, C. Sun, et al., Transfer learning improves the prediction performance of a LIBS model for metals with an irregular surface by effectively correcting the physical matrix effect, J. Anal. At. Spectrom. 36 (2021) 1441–1454, https://doi.org/10.1039/d1ja00076d.
[46] S. Shabbir, W. Xu, Y. Zhang, et al., Machine learning and transfer learning for conversion of the chemical andphysical matrix effects in the determination of alkali and alkaline earthmetals with LIBS in rocks, Spectrochim. Acta B At. Spectrosc. 194 (2022) 106478, https://doi.org/10.1016/j.sab.2022.106478.
[47] J. Hu, Y. Zou, B. Sun, et al., Raman spectrum classification based on transfer learning by aconvolutional neural network: application to pesticide detection, Spectrochim. Acta A Mol. Biomol. Spectrosc. 265 (2022) 120366, https://doi.org/10.1016/j.saa.2021.120366.
[48] C. Sun, W. Xu, Y. Tan, et al., From machine learning to transfer learning in laser-induced breakdown spectroscopy analysis of rocks for Mars exploration, Sci. Rep. 11 (2021) 21379, https://doi.org/10.1038/s41598-021-00647-2.
[49] X. Lai, H. Lin, Q. Chen, et al., Performance of the 1D standard polynomials fitting method for total phase aberration compensation in digital holographic microscopy, Optik 223 (2020) 165586, https://doi.org/10.1016/j.ijleo.2020.165586.
[50] K. Jung, T. Meerbothe, C. Cui, et al., A joint three-plane physics-constrained deep learning based polynomial fitting approach for MR electrical properties tomography, NeuroImage 307 (2025) 121054, https://doi.org/10.1016/j.neuroimage.2025.121054.
[51] Q. He, S. Tang, Y. Wang, et al., Denoising of burst vibrations by adaptive polynomial fitting in φ-OTDR, Opt. Fiber Technol. 85 (2024) 103780, https://doi.org/10.1016/j.yofte.2024.103780.
[52] H. Chen, B. Lin, K. Cai, et al., Quantitative analysis of organic acids in pomelo fruit using FT-NIR spectroscopy coupled with network kernel PLS regression, Infrared Phys. Technol. 112 (2021) 103582, https://doi.org/10.1016/j.infrared. 2020.103582.
[53] X. Huang, L. Xia, Improved kernel PLS combined with wavelength variable importance for near infrared spectral analysis, Chemom. Intell. Lab. Syst. 168 (2017) 107–113, https://doi.org/10.1016/j.chemolab.2017.06.013.
[54] Y. Seo, D. Corona, N. Hall, On the theoretical maximum achievable signal-to-noise ratio (SNR) of piezoelectric microphones, Sensors Actuators A Phys. 264 (2017) 341–346, https://doi.org/10.1016/j.sna.2017.04.001.
[55] T. Chen, L. Sun, H. Yu, et al., Online Fe grade monitoring of iron ore slurry by Morse wavelet transform and lightweight convolutional neural network based on LIBS, Spectrochim. Acta B At. Spectrosc. 210 (2023) 106821, https://doi.org/10.1016/j.sab.2023.106821.
[56] S. Yao, L. Zhang, K. Yin, et al., Identifying laser-induced plasma emission spectra ofparticlesin a gas-solid flow based on the standard deviation ofintensity across an emission line, J. Anal. At. Spectrom. 33 (2018) 1676–1682, https://doi.org/10.1039/c8ja00194d.
[57] J. Xie, M. Wang, S. Xu, et al., The unsupervised feature selection algorithms based on standard deviation and cosine similarityfor genomic data analysis, Front. Genet. 12 (2021) 684100, https://doi.org/10.3389/fgene.2021.684100.
[58] X. Zhu, P. Gu, G. Wu, Pedotransfer functions development for modeling FC and PWP using Vis-NIR spectra combined with PLSR and regression models, Vib. Spectrosc. 28 (2024) 103731, https://doi.org/10.1016/j.vibspec.2024.103731.
[59] J. Zheng, J. Lu, B. Zhang, et al., Experimental study of laser-induced breakdown spectroscopy (LIBS) for direct analysis of coal particle flow, Appl. Spectrosc. 68 (2014) 672–679, https://doi.org/10.1366/13-07278.
[60] W. Li, M. Dong, S. Lu, et al., Improved measurement of the calorific value of pulverized coal particle flow by laser-induced breakdown spectroscopy (LIBS), Anal. Methods 11 (2019) 4471, https://doi.org/10.1039/c9ay01246j.